Journal of Sustainability Science and Management
Volume 17 Number 4, April 2022: 57-69
eISSN: 2672-7226

VEGETATION INDICES OF *ACACIA MANGIUM* USING LANDSAT 8 OPERATIONAL LAND IMAGER

AQILAH NABIHAH ANUAR[1], ISMAIL JUSOH[1]* AND AFFENDI SUHAILI[2]

[1]Faculty of Resource Science and Technology (FRST), Universiti Malaysia Sarawak (UNIMAS), 94300 Kota Samarahan, Sarawak, Malaysia. [2]Forest Operation Branch, Forest Department Sarawak, Wisma Sumber Alam, Petra Jaya, 93660 Kuching, Sarawak, Malaysia.

**Corresponding author: jismail@unimas.my*
Submitted final draft: 3 January 2022 *Accepted: 21 January 2022* http://doi.org/10.46754/jssm.2022.4.005

Abstract: Monitoring a forest plantation using satellite remote sensing would be an attractive alternative compared to using a conventional method such as ground-based observations. Ground-based monitoring can be laborious and time-consuming, especially when it involves a large forested area. In contrast, satellite remote sensing can provide a synoptic view of the whole area in a single dataset. However, the ability to relate the relationship between spectral reflectance signature from Landsat 8 and the planted *Acacia mangium* is not fully understood, especially in Malaysia. This study was conducted to determine the vegetation reflectance band and indices to distinguish between *A. mangium* canopy and other land covers. Landsat 8 OLI image acquisition and analyses were performed to identify detected reflectance bands and vegetation indices (VIs) of the *A. mangium* plantation of four years old and above. Results showed that out of seven bands, only band 7 or short-wave infrared 2 is the most suitable spectral band for detecting *A. mangium* trees of age four years and older. The spatial distribution of land cover illustrated that 55.1% of the plantation area is covered with *A. mangium*. The addition of NDVI, EVI, MSAVI and ND43 improved different land cover distinguishing capabilities. The higher the values of VIs, the denser the *A. mangium* cover and the negative values illustrate less vegetation cover and open canopy within the study area. The VI shows a clear profile in which bare soil and water bodies are clearly defined against *A. mangium* canopy. A land cover map can be generated based on band 7 spectral response and VIs and provides real-time distribution of *A. mangium*. It can be used to monitor forest resources over a large area with minimal groundwork.

Keywords: *Acacia mangium* plantation, Landsat 8, spectral reflectance bands, remote sensing, vegetation indices.

Introduction

Satellite remote sensing such as Landsat has been reported to have the potential to overcome ground measurement limitations. Implementing remote sensing and geographic information system (GIS) in forestry has comprehensively allowed us to view a large forested area. Recent studies have shown that remotely sensed data have been broadly applied in monitoring and estimating biomass over a large area (Ji *et al*., 2012; Dube *et al*., 2016; Zhang *et al*., 2019; Suárez *et al.,* 2020). Landsat has also been widely used in obtaining aerial images on various types of forest cover (Foody *et al*., 2003; Lu *et al*., 2004; Günlü *et al*., 2014). Landsat 8 Operational Land Imager (OLI) is the continuation and upgraded version of the previous Landsat (Landsat TM and Landsat ETM+) (Li *et al*., 2014) that had been widely used in the study of biomass estimation (Dube & Mutangga, 2015). The aerial images downloaded from the database in the form of spectral bands such as from Landsat 5 Thematic Mapper (TM) and Landsat 7 Enhanced Thematic Mapper Plus (ETM+) have long been reported in providing relevant information for studies regarding the estimation of biomass (Kajisa *et al*., 2009; Basuki *et al*., 2013). In a study by Lu *et al*. (2004) using Landsat TM spectral bands, a high correlation was discovered between the digital data with aboveground biomass, basal area, average stand height and average stand diameter of trees from the Brazilian Amazon Basin. Their

findings, however, stated that as the forest stand structure and associated canopy shadow differ from one forest type to another, the result cannot explain the overall variation of different kinds of forest.

Landsat 8 satellite imagery used the multispectral imaging system with 11 specific spectral channels. These channels are sensitive to a narrow radiation length, thus providing the image in various greyscales of resolution cells in multilayer images (Hlatshwayo *et al*., 2019). The spectral channels involved in vegetation studies are visible light spectrum (blue, green and red), near-infrared and short-wave infrared, band 2 to band 7. These spectral channels from Landsat 8 are summarized in Table 1 (U.S. Geological Survey, 2018).

Vegetation has a unique spectral signature that makes it distinguishable from all other land covers in the visible and near-infrared spectral regions because the vegetation foliage is a good absorber of visible light. The spectral radiation detected on vegetation is low in the blue and red regions from the visible light due to the absorption of green pigments (chlorophyll) found abundantly in the palisade cells of plant leaves (Gibson, 2000). The absorption occurred mainly for photosynthesis as the green pigments absorbed energy in the wavelength centred at 0.45 μm and 0.67 μm. In the near-infrared region of the electromagnetic spectrum, ranging between 0.7 μm to 1.3 μm, the plant leaves reflected at least 50% of the energy due to the irregularity arrangement of the mesophyll cells inside the leaf (Kumar, 2005). Meanwhile, for bare soil, the spectral reflectance signature depends on the soil composition. In most cases, bare soil reflected the highest radiation. The image viewed for the area with bare soil appears to be brighter and yellowish-red (CRISP, 2020).

Satellite spectral signal has a limitation due to variation on the solar zenith angle as the satellite orbiting along the Earth's latitudinal gradient (Rouse *et al*., 1974). Hence, there had been studies conducted that introduce vegetation index (VI) to improve the limitation from Landsat reflectance bands. Normal Differences Vegetation Index (NDVI) is a mathematical transformation using band 4 (red) and band 5 (near-infrared) to eliminate the sun angle differences and minimizing the atmospheric effect. This index measures the differences in the ratio between the red reflectance band absorbed by the chlorophyll and the value of near-infrared detected after it passed through the mesophyll cell in the vegetation (Elvidge & Chen, 1995). It has been one of the most commonly and widely used VIs in many forestry and agriculture applications.

Enhance vegetation index (EVI) is another vegetation index that was used to correct the distortion from the reflected light caused by atmospheric influence and the ground under the vegetation canopy cover (Huete *et al*., 2002). The application of EVI is a reliable alternative in displaying the spatial distribution of aboveground biomass in a species-level map (Pandey *et al*., 2019). The feature of this index is that it does not become saturated when viewing an area with a thick canopy from different types

Table 1: Spectral channel features from Landsat 8 OLI

Region on the Electromagnetic Spectrum	Wavelength (μm)	Spatial Resolution	Band
Visible Light			
Blue	0.45 - 0.51	30 m	B2
Green	0.53 - 0.59	30 m	B3
Red	0.64 - 0.67	30 m	B4
Near-infrared	0.85 - 0.88	30 m	B5
Short-wave Infrared			
SWIR 1	1.57 - 1.6	30 m	B6
SWIR 2	2.11 - 2.29	30 m	B7

Source: U.S. Geological Survey (2018)

of vegetation as this index remains sensitive. Other vegetation indices, such as modified soil adjusted vegetation index (MSAVI) were proven to be helpful in biomass estimation of study by lessening the effect from the light condition, exposed soil or terrain slope effect and orientation (López-Serrano *et al*., 2016). Meanwhile, normalized difference band 4 and band 3 Index (ND43) detect green colour changes in vegetation like NDVI (Wanjura & Hartfield, 1987). The combination of band 3 green and band 4 red into this vegetation index showed relatively notable changes in terms of the greenness of the vegetation canopy.

Currently, there is little information available on the *Acacia mangium* using Landsat 8 despite the popularity of *A. mangium* being used as planting material in reforestation. *Acacia mangium* is successfully and the most extensively planted species for forest plantation in Sarawak, Malaysia (Wong *et al*., 2014; Jusoh *et al*., 2017; Adam & Jusoh, 2018). Thus, monitoring distribution and area coverage of *A. mangium* plantation has become crucial. The current paper determines the spectral reflectance bands and vegetation indices capable of distinguishing *A. mangium* canopy from other land covers.

Materials and Methods

Study Area

The study site is located in Bintulu, Sarawak, Malaysia, approximately 60 km from Bintulu town. The coordinates of the study area are N 3º 19' 56.81", E 113º 26' 37.72". The total size of planted *A. mangium* area was approximately 5,000 ha in 2016. The plantation is owned by Daiken Sarawak Sdn. Bhd. The plantation had various stand ages from four to 12 that dominated the study area when the study was conducted. The planting of *A. mangium* was conducted starting from 2002 and Figure 1 shows the progress of the plantation as of 2015.

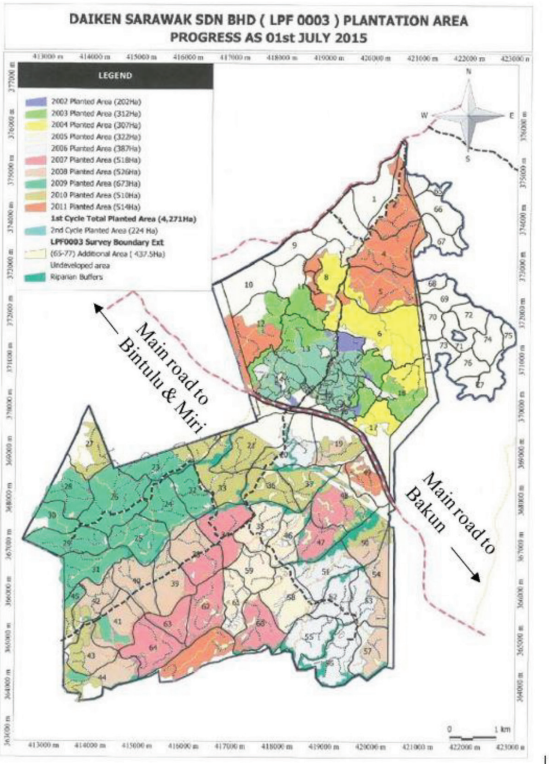

Figure 1: *Acacia mangium* plantation area as of 2015
(Adapted with permission from Daiken Sarawak Sdn. Bhd.)

The colour illustrates the year of the *A. mangium* planted while the numbers represent the number of the planting blocks on the area.

Ground Truthing

A ground-truthing was conducted along with the establishment of sampling plots for growth and biomass study between 8th and 10th March 2016. During ground-truthing locations of different *A. mangium* stand ages using Global Positioning System (GPS) were recorded. We also marked the locations of some streams, ponds, undeveloped areas and harvested areas.

Satellite Image Acquisition

One full scene of Landsat 8 of the study area located at N 3º 19' 56.81", E 113º 26' 37.72" with path 119 and row 58 from the World Reference System 2 (WRS2) was used for this study. Figure 2 shows the Landsat 8 OLI image of the area. The image (Scene ID # LC81190582016145LGN00) was acquired on 24th May 2016. The image selection was based on the study area's least cloud coverage (below 20%). The spatial resolution of the imagery is 30 x 30 m for the entire multispectral band. The metadata downloaded had all eleven spectral reflectance bands from the OLI sensor and the thermal sensor of Landsat 8 (Figure 2).

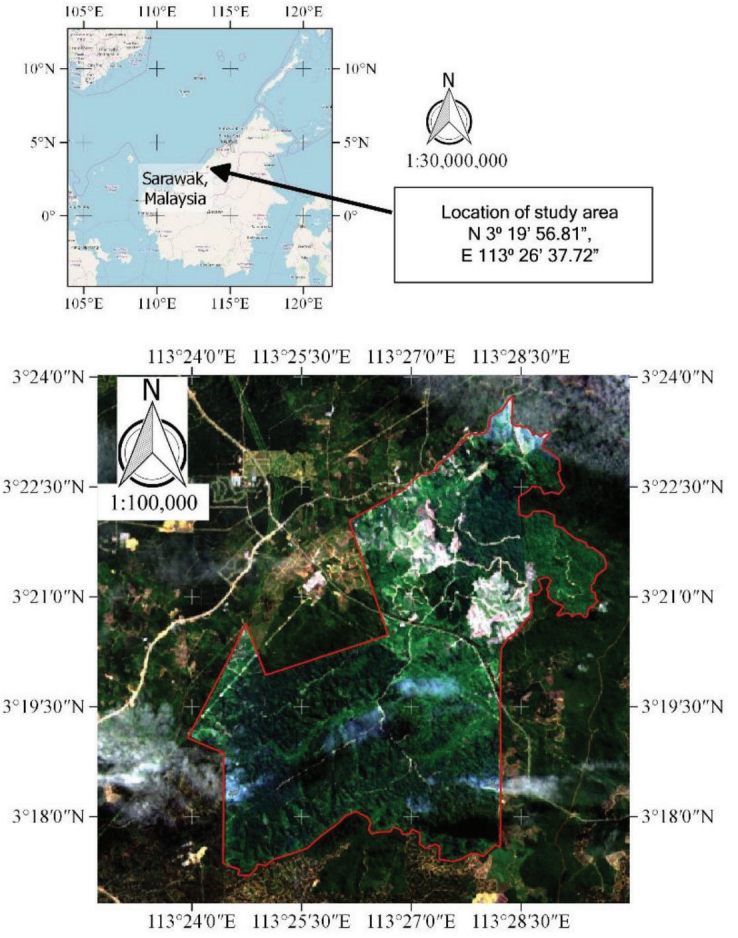

Figure 2: A satellite image on the study site from Landsat 8 OLI. The region of interest (ROI) is within the red line. Acquisition date: May 24, 2016 (USGS, 2016)

Image Pre-processing

A geometric correction was conducted on the downloaded image by setting the spatial reference coordinate reference system (CRS) of the study area fixed to WGS84 UTM Zone 49 N. The radiometric correction was performed using Dark Object Subtraction (DOS) method, converting Landsat 8 OLI digital numbers (DN) (López-Serrano *et al*., 2016). The software used was Quantum GIS ver. 2.8.5. and ArcGIS 10.4 (ESRI).

Band and Vegetation Indices (VIs)

The variables of interest were satellite bands and the VIs. There are six bands which are band 2 to band 7, from individual Landsat data (Table 1). The selection of each band was based on literature and understanding the nature and sensitivity of each selected band with the vegetation (Hagner *et al*., 2007; Chander *et al*., 2009; Roy *et al*., 2014; Mishra *et al*., 2014; Roy *et al*., 2016; Hlatshwayo *et al*., 2019). The selection of VI was based on published ratios in the literature. A visual interpretation was conducted using VI's filters to refine the identified area. The vegetation indices chosen were NDVI, EVI, MSAVI and ND43 and their equations are given in Table 2.

Supervised Image Classification

Supervised classification was done to the Landsat image, which resulted in six general land cover classifications, namely (1) riparian buffer, (2) pond, (3) *A. mangium,* (4) undeveloped areas, (5) harvested areas and (6) road. The supervised classification was done using the maximum likelihood algorithm to maintain consistency and accuracy (Hlatshwayo *et al*., 2019). Spectral angle-mapping algorithm and image segmentation were used to select the area of interest for further analysis (Blaschke, 2010; ESRI, 2019). Cloud masking was performed to remove atmospheric interference (cloud and shadow from the sun angle) on the plantation area (Congedo, 2018). Land covers on the targeted area were divided into several macro-classes (MC) and class identity (ID). Macro classes were represented by soil, targeted vegetation and non-targeted vegetation. Classes IDs were classified into six land covers.

Results and Discussion

Land Cover Classification Using Spectral Bands

The land cover classification for the study area using satellite images is shown in Figure 3. The classification map was generated using a supervised classification based on object-

Table 2: Vegetation indices used in this study

Vegetation Index	Equation	Reference
Normal Differences Vegetation Index (NDVI)	$NDVI = \frac{B5 - B4}{B5 + 4}$	Rouse *et al*., 1974
Enhance Vegetation Index (EVI)	$EVI = 2.5 * \left[\frac{(B5 - B4)}{(B5 + 6 * B4 - 7.5 * B2 + 1)}\right]$	Liu & Huete, 1995
Modified Soil Adjusted Vegetation Index (MSAVI)	$MSAVI = \frac{[(2 * B5 + 1) - \sqrt{(2 * B5 + 1)^2 - 8 * (B5 - 2 * B4)}]}{2}$	Qi *et al*., 1994
Normalized Difference Band 4 and Band 3 Index (ND43)	$ND43 = \frac{(B4 - B3)}{(B4 + B3)}$	Wanjura & Hartfield, 1987

based image analysis. The Landsat images were successfully classified into plantation cover map categorized by six classes: (1) riparian buffer, (2) pond, (3) *A. mangium*, (4) undeveloped areas, (5) bare soil (harvested area) and (6) access roads (Figure 3). The green area in the map shows the area of interest, where the area represents *A. mangium* canopy cover, view from Landsat 8 OLI. The visible *A. mangium* cover was essentially standing ages of four years and above. Recently planted *A. mangium* of fours years old and below cannot be detected. This is partly because the canopy cover is too small to distinguish between exposed or bare soil areas and partly the spectral response from band 7 of Landsat 8 is unable to discriminate *A. mangium* from other objects. The light green area shows the undeveloped areas. The areas comprised grasses, herbs, ferns, shrubs (usually refer to brush vegetation) and young or open canopy *A. mangium* stands. The sea-green coloured areas are riparian buffer. These areas are streams designated for environmental protection. The ponds are in blue colour. The area with brown colour shows the bare soil or exposed area following harvesting that had taken place. The yellow lines are the plantation access roads. Overall accuracy on the classification made was 82.7% with the Kappa hat coefficient of the agreement being 0.73. The composition of the study area which illustrated six land cover classes is presented in Table 3.

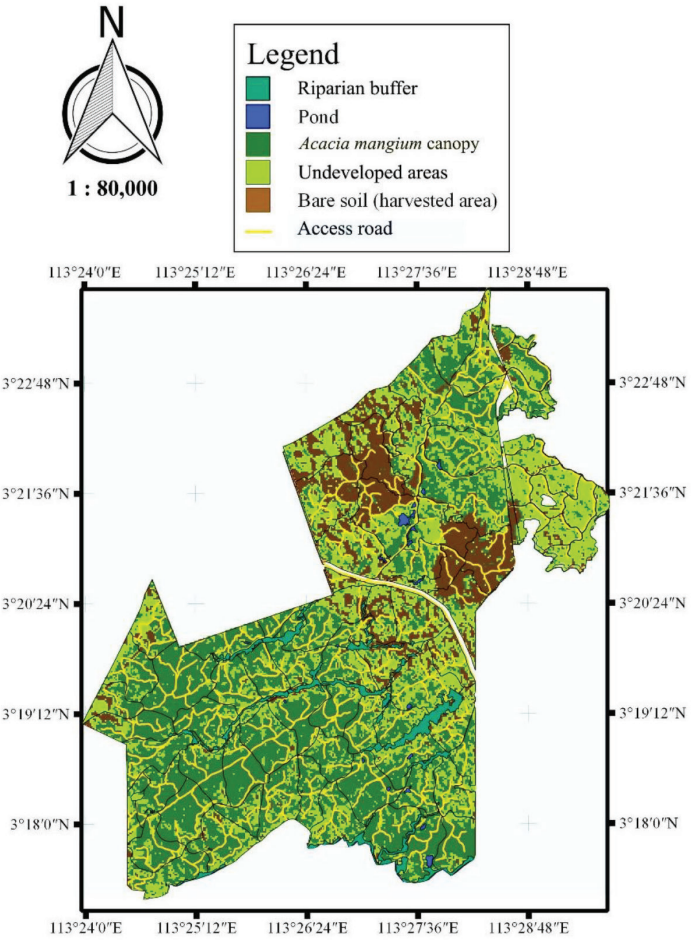

Figure 3: Land cover map of the *Acacia mangium* plantation produced by supervised classification of Landsat 8 imagery

Table 3: Summary and percentage of the classified major land cover

Land Cover Class	No. of Pixels	Total Area (ha)	Percentage (%)
Riparian buffer	1,821	163.9	3.3
Pond	219	19.7	0.4
Acacia canopy cover	30,703	2,763.3	55.1
Undeveloped areas	12,503	1,114.0	22.4
Bare soil - harvested area	9,545	859.0	17.1
Access road	931	83.8	1.7
Total area of plantation	55,722	5,003.7	100.0

The total area of the plantation determined from 55,722 total pixels was 5,003.7 ha (Table 3). The area covered with *A. mangium* was approximately 30,703 pixels, representing 2756.8 ha or 55.1% of the area. The rest of the area in the plantation was covered by streams, ponds, riparian and undeveloped zone (1,309.6 ha), equivalent to 26.1%, bare soil with 12.7% and 6.1% made up of the harvested area and road and landing areas combined, respectively.

The classes were distinguished based on the differences in the spectral responses. Table 4 shows the spectral response ranges of stream, pond, *A. mangium* cover, undeveloped and bare soil land cover classes. Every channel on the reflectance bands (band 2 – band 7) has a specific spectral response range. The spectral responses from bands 2 to 6 ranged from 0.461 to 1.600, so the six target land covers are not well separated. The six land covers: Stream, pond, *A. mangium* cover, undeveloped areas, harvested areas and roads are not distinguishable using band 2 to band 6.

Band 7 was the best spectral parameter for separating between *A. mangium* canopy and other land covers. The spectral responses of stream, pond, *A. mangium* cover, undeveloped areas and bare soil, from band 7 were discontiguous, making the land covers distinct as shown in Figure 3. The spectral signature detected from vegetation was the product after electromagnetic energy interacting with the leaves, down to the level of its cellular structures (Gausman *et al*., 1969). Interactions between electromagnetic energy, especially on the blue and red regions in visible light and chlorophyll *a, b*, β-carotene and other components inside the leaf pigment made the spectral signatures unique between different species of vegetation.

Table 4: Spectral response ranges of stream, pond, *Acacia mangium*, undeveloped area, harvested area and bare roads obtained from spectral band 2 to band 7 Landsat 8 Operational Land Imager

Spectral Band	Spectral Response of Stream (µm)	Spectral Response of Pond (µm)	Spectral Response of *Acacia mangium* Canopy (µm)	Spectral Response of Undeveloped Area (µm)	Spectral Response of Harvested Area (µm)	Spectral Response of Road (µm)
B2 (Blue)	0.461−0.629	0.461−0.629	0.461−0.467	0.463−0.465	0.467−0.482	0.45−0.475
B3 (Green)	0.544−0.556	0.542−0.560	0.544−0.555	0.547−0.555	0.551−0.575	0.540−0.571
B4 (Red)	0.645−0.650	0.640−0.658	0.644−0.648	0.645−0.646	0.640−0.670	0.649−0.667
B5 (NIR)	0.850−0.863	0.851−0.863	0.864−0.878	0.874−0.881	0.866−0.872	0.855−0.870
B6 (SWIR1)	1.581−1.591	1.575−1.586	1.580−1.591	1.585−1.591	1.598−1.600	1.590−1.600
B7 (SWIR2)	2.150−2.196	2.130−2.200	2.148−2.187	2.166–2.190	2.241−2.290	2.218−2.288

Our study showed that band 7 was significantly effective in distinguishing different land cover types, even on areas covered in vegetation. Band 7 (short-wave infrared 2) is relatively sensitive to water content. A study on distinguishing the different species of vegetation based on the amount of water present within the spongy mesophyll tissue and cavities of the leaf from band 7 had shown a positive result (Gausman *et al*., 1969). As band 7 is sensitive to moisture content, equivalent water thickness (EWT) within the canopy layer could also explain why *A. mangium* was distinguishable compared to other vegetation species (Ceccato *et al*., 2001; Asif *et al*., 2017).

Land Cover Classification Using Vegetation Indices

The use of vegetation indices could improve the spectral signatures in identifying targets than when using a single reflectance band. Adding vegetation indices in defining the boundaries for areas representing *A. mangium* canopy cover, bare soil and undeveloped zones are more significant as the boundaries become more visible and prominent. Our results showed that NDVI, EVI, MSAVI and ND43 could distinguish the specified land cover targets (Table 5). The Landsat 8 image classified into the land cover using four VIs (NDVI, EVI, MSAVI and ND43) is shown in Figure 4.

The land cover classification using VIs in the filter refines the boundary on *A. mangium* even more. This is due to the use of the green tone from the image. The pattern of the arrangement viewed from the image and texture produces the impression of a homogenous spectral signature of *A. mangium* canopy cover due to the morphological characteristic of *A. mangium* itself. *Acacia mangium* canopy is evergreen, covered with branchlets that hold the phyllodes in acutely triangle position (Sein & Mitlöhmer, 2011).

The NDVI is widely used for vegetation studies because it is sensitive to green vegetation, even for vegetation at low coverage. The NDVI value ranges from −1 to 1, where a negative value indicates a non-vegetated area (Table 5). Figure 4 (a) shows that higher forest density was found at the southern portion of the plantation and the range of NDVI between 0.70 and 0.85. The higher the value, the darker the green colour showing dense *A. mangium* cover for the lower the value with brown and red shows less *A. mangium* cover. The yellow colour shows areas with shrubs, bushes and treelet (brush forest) and young *A. mangium* stands. The northern region shows a large tract with white colour, which are mixed areas of open, undeveloped was excluded from NDVI mapping because the vegetation of interest was not there.

The EVI was introduced by modifying the NDVI as it corrected the red band for atmospheric aerosol scattering using the blue band (Silleos, 2006). This VI is useful for enhancing sensitivity to a region with higher biomass and reducing atmospheric influence while improving vegetation monitoring through

Table 5: Vegetation indices spectral range detected from *Acacia mangium* canopy cover, undeveloped zone and bare soil

Vegetation Index (VI)	Spectral Range of Stream (µm)	Spectral Range of Pond (µm)	Spectral Response of *Acacia mangium* Canopy (µm)	Spectral Response of Undeveloped Area (µm)	Spectral Response of Harvested Area (µm)	Spectral Response of Road (µm)
NDVI	0.158−0.386	0.140−0.450	0.706−0.823	0.834−0.868	0.380−0.653	0.306−0.636
EVI	0.090−0.250	0.181-0.213	0.415−0.678	0.640−0.753	0.294−0.467	0.210−0.467
MSAVI	-0.165−0.168	0.009−0.235	0.355−0.625	0.584−0.681	0.180−0.420	0.195−0.416
ND43	-0.530−0.006	-0.244−-0.162	0.034−0.061	-0.244−-0.162	0.040−0.180	0.017−0.207

a de-coupling of canopy background signal (Huete *et al*., 2002). Figure 4 (b) shows the range of EVI between 0.41 and 0.66 and higher values indicate higher biomass, lower values show less biomass. Mapping using EVI (Figure 4 (b)) shows the variation of biomass distribution within the plantation because it is more sensitive than NDVI. The darker the green colour, the higher the biomass. EVI can display spatial distribution in a species-level map (Pandey *et al*., 2019).

The SAVI is able to minimize soil brightness, thus, minimizing the effect of soil background. In comparison, MSAVI was developed to enhance SAVI and correct the red and near-infrared (band 5) flux (Silleos, 2006) and as well as reducing the influence of bare soil in SAVI (Xue & Su, 2017). The result is to increase vegetation signal to soil noise ratio (Qi *et al*., 1994). This is done to minimize the effect of bare soil on the SAVI and this helps when applied to areas with a high level of exposed soil surface. As shown in Figure 4 (c), MSAVI refined the *A. mangium* area. Range of MSAVI was between 0.35 and 0.65. The higher the values, the denser the *A. mangium* cover while the lesser the values mean, the more open the canopy.

Figure 4 (d) shows the range of ND43 between −0.69 and 0; the negative values (0 or less) show less dense vegetation cover or *A. mangium* canopy open. An area with a positive value show dense or closed canopy *A. mangium*. This VI could redefine the road clearer even from the vegetation canopy. This index showed *A. mangium* tree density was scattered in the study area showing relatively less *A. mangium* density in the southern part, which was not shown in the NDVI map. The combination of band 3 (green) and band 4 (red) into this vegetation index

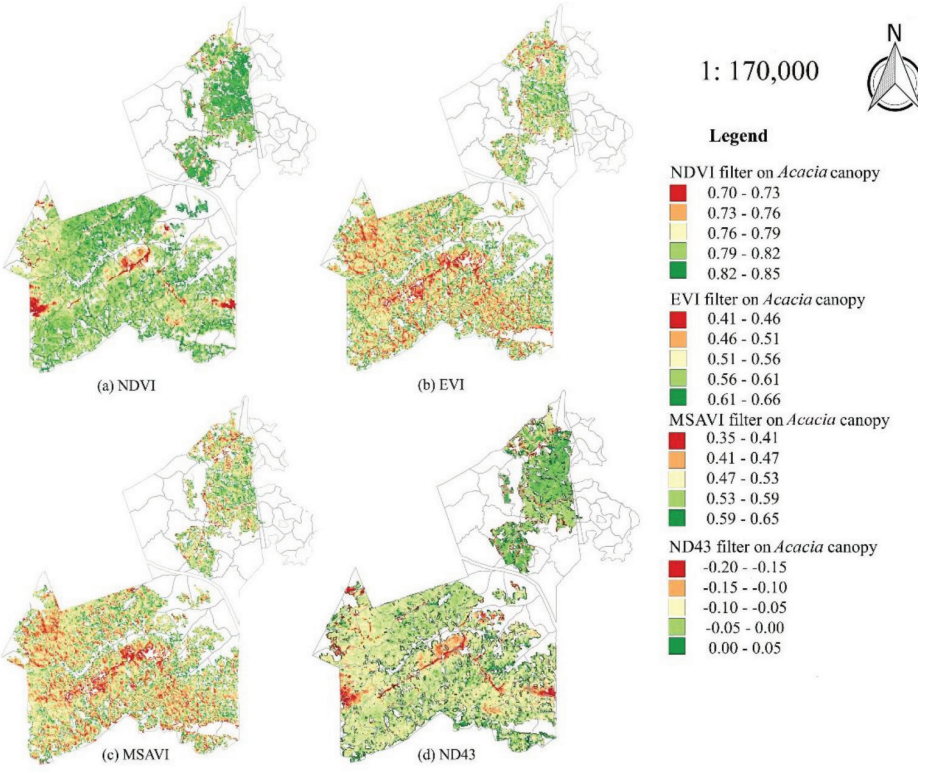

Figure 4: Maps of vegetation indices extracted from Landsat 8 showing *A. mangium* plantation area (a) NDVI, (b) EVI, (c) MSAVI and (d) ND43

showed relatively notable changes in terms of the greenness of the vegetation canopy, hence being able to distinguish the road even under thick canopy cover.

Adding vegetation indices into this study area showed significant improvement in identifying the area with *A mangium*. Studies have shown that vegetation indices helped minimize the atmospheric effects and improved the relationship between Landsat data and aboveground biomass. According to Huete *et al*. (2002) each pixel fully belongs to a set of discretion and mutually exclusive classes. By imparting vegetation indices into the filtering stage, the redefining boundary of *A. mangium* was effectively conducted. Our study showed that the area with *A. mangium* was refined using the EVI filter down to its one-pixel size compared to the NDVI filter. Enhanced vegetation index (EVI) appeared to be more sensitive than NDVI and thus strictly assigns the pixels in discrete classes in the display (Lijun *et al.,* 2008). NDVI tends to be homogenously saturated in an area with dense vegetation while EVI retained its sensitivity even under the heavily vegetated area (Huete *et al*., 2002). This study shows that the ND43 vegetation index helps redefine the road despite the area concealed behind the canopy cover of *A. mangium*.

Conclusion

Our study showed the capability of utilizing Landsat 8 OLI in detecting and determining the distribution of *A. mangium* trees of four years old and above. The most significant spectral signature detected for *A. mangium* is band 7 (short-wave infrared 2). A land cover map can be produced based on this spectral signature using supervised classification techniques and estimated acreage of *A. mangium* can be estimated. The addition of vegetation indices improved the distinguishing capability of different land covers. Vegetation indices such as NDVI, EVI, MSAVI and ND43 distinguished areas with *A. mangium* canopy cover from areas with other land covers present in the plantation area. Hence, large-scale forest plantations can map and monitor their timber resources accordingly on a real-time basis with minimal ground operations, which are time-consuming and costly. Although this study demonstrates the utility of NDVI, EVI, MSAVI and index ND43 on *A. mangium* canopy, additional research is needed to substantiate our findings at various plantation sites in Sarawak, Malaysia.

Acknowledgements

We would like to express our gratitude and gratefully acknowledge Daiken Sarawak Sdn. Bhd. for the permission to use their plantation as the study site. We thank Mr. Friendie Su and his crew for their cooperation and assistance in all phases of the fieldwork. We are grateful to the Ministry of Higher Education Malaysia for the financial support under the Fundamental Research Grant Scheme FRGS/1/2017/WAB07/UNIMAS/02/1.

References

Adam, N. S., & Jusoh, I. (2018). Allometric model for predicting aboveground biomass and carbon stock of *Acacia* plantation in Sarawak, Malaysia. *Bioresources, 13*(4), 7381-7394.

Asif, M. J., Govender, N. T., Ang, L. H., & Ratman, W. (2017). Growth performance and lignin content of *Acacia mangium* Willd. and *Acacia auriculiformis* A. Cunn. ex Benth. under normal and stressed conditions. *Journal of Forest Science*, *63*(8), 381-392. Doi: 10.17221/100/2015-JFS

Basuki, T. M., Skidmore, A. K., Hussin, Y. A., & Van Duren, I. (2013). Estimating tropical forest biomass more accurately by integrating ALOS PALSAR and Landsat-7 ETM+ data. *International Journal of Remote Sensing*, *34*, 4871-4888.

Blaschke, T. (2010). Object based image analysis for remote sensing. *ISPRS Journal of Photogrammetry and Remote Sensing, 65*, 2-16.

Ceccato, P., Flasse, S., Tarantola, S., Jacquemoud, S., & Grégoire J. M. (2001). Detecting vegetation leaf water content using reflectance in the optical domain. *Remote Sensing of Environment, 77*(1), 22-33. https://doi.org/10.1016/S0034-4257(01)00191-2.

Centre for Remote Imaging, Sensing and Processing (CRISP). (2001). *Principal of remote sensing*. http://www.crisp.nus.edu.sg/~research/tutorial/rsmain.htm.

Chander, G., Markham, B. L., & DL Helder, D. L. (2009). Summary of current radiometric calibration coefficients for Landsat MSS, TM, ETM+ and EO-1 ALI sensors. *Remote Sensing of Environ.*, *113*(5), 893-903. https://doi.org/10.1016/j.rse.2009.01.007

Congedo, L. (2018) Semi-automatic Classification Plugin Documentation Release 6.0.1.1, 8; doi: 10.13140/RG.2.2.29474.02242/1.

Dube, T., & Mutanga, O. (2015). Investigating the robustness of the new Landsat-8 Operational Land Imager derived texture metrics in estimating plantation forest aboveground biomass in resource constrained areas. *ISPRS Journal of Photogrammetry and Remote Sensing*, *108*, 12-32.

Dube, T., Mutangga, O., Cletah, S., Adelabu, S., & Tsitsi, B. (2016). Remote sensing of aboveground forest biomass: A review. *Tropical Ecology*, *57*(2), 125-132

Elvidge, C. D., & Chen, Z. (1995). Comparison of broad-band and narrow-band red and near-infrared vegetation indices. *Remote Sensing of Environment, 54,* 38-48.

ESRI. (2016). *ArcMap.* http://desktop.arcgis.com/en/arcmap/.

Foody, G. M., Boyd, D. S., & Cutler, M. E. J. (2003). Predictive relations of tropical forest biomass from Landsat TM data and their transferability between regions. *Remote Sensing of Environment, 85*(4), 463-474. https://doi.org/10.1016/S0034-4257(03)00039-7

Gausman H. W., Allen W. A., Myer V. I., & Cardenas R. (1969), Reflectance and internal structure of cotton leaves. *Gossypium hirsutum* L. *Agronomy Journal, 61*, 374 - 376.

Gibson, P. J. (2000). *Introductory remote sensing: Principles and concepts*. London: Routledge.

Günlü, A., Ercanli, I., Baskent, E. Z., & Cakir, G. (2014). Estimating aboveground biomass using Landsat TM imagery: A case study of Anatolian Crimean pine forests in Turkey. *Annals of Forest Research, 57*(2), 289-298. DOI: 10.15287/afr.2014.278

Hagner, O., & Reese, H. (2007). A method for calibrated maximum likelihood classification of forest types. *Remote Sensing of Environment*, *110*(4), 438- 444.

Hlatshwayo S. T., Mutanga, O., Lottering, R. T., Kiala, Z., & Ismail, R. (2019). Mapping forest aboveground biomass in the reforested Buffelsdraai landfill site using texture combinations computed from SPOT-6 pan-sharpened imagery. *International Journal of Applied Earth Observation and Geoinformation, 74*, 65-77.

Huete, A., Didan, K., Miura, T., Rodriguez, E. P., Gao, X., & Ferreira, L. G. (2002). Overview of the radiometric and biophysical performance of the MODIS vegetation indices. *Remote Sensing of Environment, 83*, 195-213.

Ji, L., Wylieb, B. K., Nossovc, D. R., Petersona, B., Waldropd, M. P., McFarlandd, J. W., Roverb, J., & Hollingsworthe, T. N. (2021). Estimating aboveground biomass in interior Alaska with Landsat data and field measurements International. *Journal of Applied Earth Observation and Geoinformation 18*, 451-461.

Jusoh, I., Suteh, J. K., & Adam, N. S. (2017). Growth and yield of *Acacia mangium* based on permanent sampling plots in a plantation.

Transactions on Science and Technology, 4(4), 513-518.

Kajisa, T., Murakami, T., Mizoue, N., Top, N., & Yoshida, S. (2009). Object-based forest biomass estimation using Landsat ETM+ in Kampong Thom Province, Cambodia. *Journal of Forest Research*, *14*, 203-211.

Kumar, D. N. (2005). *Basics of Remote Sensing and GIS*. New Delhi: Laxmi Publication (P) Ltd. Pp 14 - 30.

Li, P., Jiang, L., & Feng, Z. (2014). Cross-comparison of vegetation indices derived from Landsat-7 Enhanced Thematic Mapper Plus (ETM+) and Landsat-8 Operational Land Imager (OLI) sensor. *Remote Sensing*, *6,* 310-329

Lijun, Z.., Zeng-Xiang, Z., Ting-ting, D., & Xia, W. (2008). Application of MODIS/NDVI and MODIS EVI to extracting the information of cultivated land and comparison analysis. *Transactions from the Chinese Society of Agriculture and Engineering, 2008*, 167-172. http//:DOI:10.3969/j. issn.1002-6819.2008.3.033.

Liu, H. Q., & Huete, A. (1995). A feedback based modification of the NDVI to minimize canopy background and atmospheric noise. *IEEE Transactions on Geoscience and Remote Sensing*, *33*(2), 457-465. https:// doi 10.1109/TGRS.1995.8746027

López-Serrano, P. M., Corral-Rivas, J. J, Díaz-Varela, R. A., Álvarez-González, J. G., & López-Sánchez, C. A. (2016). Evaluation of radiometric and atmospheric correction algorithms of aboveground forest biomass estimation using Landsat 5 TM data. *Remote Sensing, 8*(5)*,* 1-19. https://doi.org/10.3390/rs8050369

Lu, D., Mausel, P., Brondı´zio, E., & Mora, E. (2004). Relationships between forest stand parameters and Landsat TM spectral responses in the Brazilian Amazon Basin. *Forest Ecology and Management, 198*, 149-167. https//:doi.org/10.1016/j.foreco.2004.03.048, p. 11-66.

Mishra, N., Haque, M. O., Leigh, L., Aaron, D., Helder, D., & Markham, B. (2014). Radiometric cross calibration of Landsat 8 operational land imager (OLI) and Landsat 7 enhanced thematic mapper plus (ETM+). *Remote Sensing*, *6*(12), 12619-12638.

Pandey, P. C., Anand, A., & Srivastava, P. K. Biodivers Conserv. (2019). Spatial distribution of mangrove forest species and biomass assessment using field inventory and earth observation hyperspectral data. *Biodiversity and Conservation, 28*(335), 1-20. https://doi.org/10.1007/s10531-019-01698-84.

Qi, J., Chehbouni, A., Huete, A. R., Kerr, Y., & Sorooshian, S. (1994). A modified soil adjusted vegetation index. *Remote Sensing of Environment*, *48*(2), 119- 126. doi. org/10.1016/0034-4257(94)90134-1

Rouse, J. W., Haas, R. H. J., Schell, J. A., & Deering, D. W. (1974). Monitoring vegetation systems in the Great Plains with ERTS. *Third ERTS Symposium, 1*, 48-62.

Roy, D. P., Kovalskyy, V., Zhang, H., Vermote, E. F., Yan, L., Kumar, S., & Egorov, A. (2016). Characterization of Landsat-7 to Landsat-8 reflective wavelength 224 and normalized difference vegetation index continuity. *Remote Sensing of Environment*, *185*, 57-70.

Roy, D. P., Wulder, M., Loveland, T. R., Woodcock, C., Allen, R. anderson, M., . . . Kennedy, R. (2014). Landsat-8: Science and product vision for terrestrial global change research. *Remote Sensing of Environment*, *145*, 154-172.

Sein, C. C., & Mitlohmer, R. (2011). *Acacia mangium* Willd. Ecology and silviculture in Vietnam. Indonesia: Center for International Forestry Research (CIFOR). West Bogor, Indonesia, 2011, p. 1-3.

Silleos, N. G., Alexandridis, T. K., Gitas, I. Z., & Perakis, K. (2006). Vegetation indices: Advances made in biomass estimation and vegetation monitoring in the last 30 years. *Geocarto International*, *21*(4), 21-28.

Suárez, J. C., Smith, S., Bull, G., Malthus, T. J., D Donoghue, D., & Knox, D. (2020). The use of remote sensing techniques in operational forestry. http://www.forestry.gov.uk/forestsat.

U.S. Geological Survey. (2018). What is Landsat and where does it begin? https://landsat.usgs.gov/what-landsat-and-when-did-it-begin. Wanjura, D. F., & Hatfield, J. L. (1987). Sensitivity of spectral vegetative indices to crop. *Transactions of ASAE*, , DOI: 10.13031/2013.30479@1987

Wong, K. S., Ahmad, H. S., Bauk, R. A., Razali, B. B., & Bujang, A. W. (2014). The essential roles of forest plantations toward sustainability of wood production and wood-based industries in Sarawak [Paper Presentation]. *The 17th Malaysian Forestry Conference: A Century of Forest Management: Lessons Learnt and the Way Forward*. 11-12 November, Kota Kinabalu, Sabah. 2014; pp.16.

Xue, J., & Su, B. (2017). Significant remote sensing vegetation indices: A review of developments and applications. *Journal of Sensors*, https//:doi.org/10.1155/2017/1353691

Zhang, J., Lu, C. Xu, H. & Wang, G. (2019). Estimating aboveground biomass of Pinus densata-dominated forests using Landsat time series and permanent sample plot data. *J. For. Res.*, *30*(5), 1689-1706. https://doi.org/10.1007/s11676-018-0713-7